Microscopy AND
Microanalysis

Original Article

Coupling Secondary Ion Mass Spectrometry and Atom Probe Tomography for Atomic Diffusion and Segregation Measurements

Alain Portavoce[1]*, Khalid Hoummada[2] and Lee Chow[3]

[1]CNRS, IM2NP UMR 7334, 13397 Marseille, France; [2]Aix-Marseille University, IM2NP UMR 7334, 13397 Marseille, France and [3]Department of Physics, University of Central Florida, Orlando, Florida 32816, USA

Abstract

For a long time, secondary ion mass spectrometry (SIMS) was the only technique allowing impurity concentrations below 1 at% to be precisely measured in a sample with a depth resolution of few nanometers. For example, SIMS is the classical technique used in microelectronics to study dopant distribution in semiconductors and became, after radiotracers were forsaken, the principal tool used for atomic transport characterization (diffusion coefficient measurements). Due to the lack of other equivalent techniques, sometimes SIMS could be used erroneously, especially when the analyzed solute atoms formed clusters, or for interfacial concentration measurements (segregation coefficient measurements) for example. Today, concentration profiles measured by atom probe tomography (APT) can be compared to SIMS profiles and allow the accuracy of SIMS measurements to be better evaluated. However, APT measurements can also carry artifacts and limitations that can be investigated by SIMS. After a summary of SIMS and APT measurement advantages and disadvantages, the complementarity of these two techniques is discussed, particularly in the case of experiments aiming to measure diffusion and segregation coefficients.

Key words: atom probe tomography, atomic diffusion, grain boundary segregation, secondary ion mass spectrometry

(Received 19 July 2018; revised 5 November 2018; accepted 16 November 2018)

Introduction

Secondary ion mass spectrometry (SIMS) is a primary technique allowing for quantitative measurement of impurity concentration in materials at the nanometric scale. During measurement, a primary ion beam (Cs^+, O_2^+ etc.) is used to sputter the sample while a small fraction of the sample atoms (<1%) that are ionized during this process (secondary ions) is collected. The mass of these ions is then determined using a mass analyzer (Benninghoven et al., 1987). Dynamic (D) SIMS (the most common) allows one-dimensional (1D) concentration profiles of a selected impurity to be measured in material bulk with a sub-nanometer depth resolution, using a sector field mass analyzer. D-SIMS is widely used to determine diffusion profiles of impurities (concentrations lower than 1%) in materials. Nanoscale (nano) SIMS, which also uses a magnetic sector mass analyzer with multicollection (parallel collection of 5–7 different ionic species using 5–7 different detectors), allows 2D imaging with high-resolution spatial analysis (of the order of 50 nm) thanks to the scanning of the sample surface with a microprobe. Nano-SIMS is often used to determine 2D maps of impurity concentration variations in materials, such as concentration variations due to impurity segregation on extended defects such as grain boundaries (GBs). Time-of-flight (TOF) SIMS is more appropriate for 2D surface analysis or depth profiling in the near surface region. The TOF technique does not produce quantitative analyses (semi-quantitative), but allows the simultaneous analysis (2D mapping) of any element isotope on the sample surface. SIMS is a destructive technique since a crater is created in the sample during analysis, and needs a smooth surface for good depth resolution (the surface roughness being mostly amplified during sputtering). Quantitative SIMS analysis is generally dedicated to the measurement of concentrations lower than 1 at% due to matrix effects. For D-SIMS, the size of the probed area is in the hundreds of micrometers squared and the detection limit is about 10^{15} to 10^{16} at/cm^3 (0.02–0.2 ppm). The SIMS signal needs a reference sample for concentration calibration. The two main SIMS aberrations are the matrix and the mixing effects. The matrix effect is related to the variation of the ionization yield of the elements versus the sample bulk concentration (or sometimes the crystallographic orientation) (Saha & Chakraborty, 2013). In this case, the SIMS signal is no longer proportional to the analyzed element concentration and cannot be simply calibrated using a reference sample. Usually, these analysis conditions occur for concentrations larger than 1 at%, limiting the use of SIMS for impurity concentration measurements. However, the ionization yield is generally not significantly different between isotopes, allowing high concentration profiles of matrix isotopes to be measured by SIMS (Südkamp et al., 2013). The mixing effect is related to the ion-beam mixing induced in the sample by the sputtering process, leading to distortions in the measured concentration profile (Zalm & Vriezema, 1992; Portavoce et al., 2009). D-SIMS measurements correspond to a large area (analyzed region of tens to hundreds of micrometer square) and

*Author for correspondence: Alain Portavoce, E-mail: alain.portavoce@im2np.fr

allow the measurement of deep concentration profiles (up to several micrometers if needed).

Atom probe tomography (APT) allows the atomic scale 3D reconstruction of a small volume (typically $\sim 100 \times 100 \times 100$ nm^3) of the sample (Larson et al., 2013). During the analysis, the ionized atoms of the sample (shaped as a tip with a tens-of-nanometers radius) are sequentially field evaporated, in order to determine their spatial coordinates in the sample and their mass. About 50% of the atoms contained in the sample are detected and can be used to determine the 3D atomic distribution in the evaporated sample. With the exception of complex cases, such as materials made of several phases or elements with significant evaporation field differences preventing APT experimental conditions free of evaporation/reconstruction aberrations to be found, APT allows direct concentration measurements (no need for calibration, no matrix effect, no mixing effect) in the three directions of space. The sample being defined as atoms distributed in a 3D volume, APT allows numerous statistical analyses to be performed in the reconstructed volume. It is a destructive technique since the sample needs to be shaped into a tip, usually by focused ion beam (FIB) milling, before being atomically evaporated (Larson et al., 2013). Despite the high detection yield (about 50%), the APT detection limit ($\sim 10^{18}$–5×10^{19} at/cm^3) is lower than that of SIMS due to the limited size of the analyzed volumes. APT can suffer from numerous aberrations, mainly related to evaporation field effects, such as local magnification or evaporation between electrical or laser pulses (Vurpillot et al., 2000; Sha & Cerezo, 2005).

APT has already been used to study atomic transport (Kresse et al., 2013; Toyama et al., 2014; Mühlbacher et al., 2015; Aboulfadl et al., 2019), and combining SIMS and APT measurements has already been shown to be beneficial for measuring narrow distributions of solutes located close to an interface, aberrations being of different nature for these two techniques (Ronsheim et al., 2008). Due to the small sizes of the analyzed volumes, and due to the (atomic) scale of APT data, APT cannot offer the same statistics as SIMS. However, as SIMS measurements provide the global atomic distribution, and APT measurements provide localized atomic sub-distributions in the sample (in extended defects for example), SIMS and APT together can provide an interesting outlook on the chemical distribution in samples (Martinez et al., 2011). In this paper, the benefit of coupling SIMS and APT measurements is discussed in the case of materials containing atomic clustering and/or extended defects such as GBs in polycrystalline materials, in particular when studying atomic diffusion and atomic segregation. When possible, scanning transmission electron microscopy high-angle annular dark-field (STEM-HAADF) imaging was also compared to SIMS and APT profiles. This technique allows the heavy element distribution to be determined in cross-sectional samples, since the STEM-HAADF intensity is proportional to the mean atomic number $Z^{1.5}$ along the projection (Yan et al., 1998). The STEM-HAADF signal is not quantitative, but should be proportional to composition. Furthermore, STEM-HAADF profiles should not have aberrations comparable to those of SIMS or APT profiles.

Materials and Methods

In the current paper, the impurity diffusion sources were created either by implantation in the bulk of the samples or by deposition on the surface of the samples. Most implantations were performed using commercial implanters, unless otherwise indicated, and

layer deposition was performed using a commercial magnetron sputtering system. For example, the W and the Ga sources were implanted in Si(001) (De Luca et al., 2014) and Ge(001) (Luo et al., 2018), respectively. The Pt source was implanted in a polycrystalline Ni$_2$Si layer grown by reactive diffusion. The Ge source was implanted in a nano-crystalline Si layer grown by chemical vapor deposition (Portavoce et al., 2008). SIMS measurements were performed using a CAMECA IMS 3F or IMS 7F system, using either an O$_2^+$ or O$^+$ primary ion beam exhibiting energies between 3 and 10 keV. The size of the analyzed area was between 30 and 60 μm^2, and the analysis depth was measured using a KLA Tencor AlphaStep IQ profiler. The SIMS crater roughness after analysis was checked using a 3D Profiler (maximum roughness <34 nm). Sample preparation for APT analysis was performed using a FEI Helios 600 Nanolab FIB microscope. The distance between the SIMS crater and the region lifted-out for APT measurements on the same sample was between 0.3 and 1 cm. A Ni protection film was deposited at room temperature by magnetron sputtering on the samples before being processed by FIB (Portavoce et al., 2014). APT analyses were performed using a CAMECA LEAP 3000X-HR microscope in the pulsed laser mode. The analyses were carried out between 20 and 70 K, with a laser pulse frequency of 100 kHz, using a laser power between 0.15 and 1.2 nJ and an average detection rate of two ions per 1,000 laser pulses.

Precise sample fabrication and impurity implantation conditions, as well as SIMS and APT measurement conditions for each studied case can be found in the cited references.

Results and Discussion

The common method used to determine diffusion coefficients in solid materials is based on the measurement of 1D concentration profiles (Portavoce et al., 2012b). The diffusion profiles are fitted using a model (Portavoce et al., 2004b, 2010, 2012a, 2012b; De Luca et al., 2014) in which the diffusion coefficient is a parameter that is adjusted in order to get the best fit between the simulated and the experimental diffusion profiles. The experimental profile can be reproduced either using a numerical simulation (Portavoce et al., 2010, 2012a, De Luca et al., 2014) or using the solution of the diffusion equation corresponding to the appropriate diffusion annealing conditions (Mehrer, 2007; Portavoce et al., 2008). In either approach, the accuracy of the experimental profiles is of primary importance. For atomic diffusion corresponding to atomic transport of diluted elements in a given matrix (dilute solid solution), D-SIMS is currently the main technique used to measure diffusion profiles with the aim of determining "diffusion coefficients" (different from "intrinsic diffusion coefficients" in highly-concentrated solid solutions).

For example, Figure 1 presents W diffusion profiles measured by SIMS in a Si(001) substrate (De Luca et al., 2014). The initial W distribution before diffusion annealing is shown using (red) solid squares, exhibiting a quasi-Gaussian shape with a maximum concentration located at a depth of ~ 60 nm. After annealing, the maximum concentration of the W distribution shifts toward the surface and the W distribution shape becomes almost linear on a logarithmic scale. According to these observations, W atoms did not cluster since all the W atoms diffused during annealing, and W diffusion does not correspond to Fick diffusion. However, Figure 2 shows the superimposition of the SIMS profile (solid squares) measured in the sample annealed at 837°C for 48 h, with the concentration profile measured by APT (solid line)
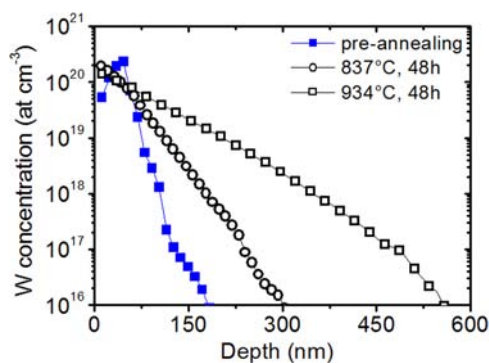
Fig. 1. Tungsten SIMS profiles measured in Si(001) wafers implanted with a W^+ ion dose of 10^{15} ions/cm^2 using a beam energy of 165 keV and annealed at 837 and 934°C for 48 h (De Luca et al., 2014).
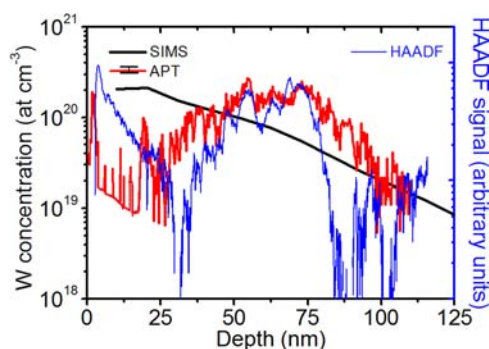

Fig. 2. Comparison between SIMS (black) and APT (red) W concentration profiles (left axis) and the HAADF intensity (blue, right axis) measured in the same Si(001) substrate implanted with a W^+ ion dose of 10^{15} ions/cm^2 and annealed at 837°C for 48 h (De Luca et al., 2014). The SIMS profile is also presented in Figure 1. The maximum error in the APT profile is superimposed (in black) on the APT legend.

and the STEM-HAADF intensity (open circles) measured on a cross-section of the same sample. The HAADF intensity is in good agreement with the APT profile, showing a Gaussian distribution of W atoms located at the same depth as the maximum concentration of the initial Gaussian distribution (before diffusion, Fig. 1). This distribution, not observed in the SIMS profile, corresponds to W clusters that have formed during the diffusion annealing. The clusters are well resolved in APT volumes as well as in high resolution (HR)-TEM and STEM-HAADF images (De Luca et al., 2014). The SIMS discrepancy is probably due to a matrix effect between bulk Si and the W-rich clusters, suggesting a lower W ionization yield in the clusters. In this example, APT measurements were used to select the accurate SIMS profiles that could be successfully used to determine the W diffusion mechanism and the W diffusion coefficient in Si (De Luca et al., 2014).

Figure 3 presents two Ga diffusion profiles (650°C for 7 days—open circles, and 750°C for 3 h—open squares) measured by SIMS on a Ge(001) substrate. After diffusion, the Ga distribution shows a "bump" centered on the maximum concentration of the initial profile (before diffusion, open triangles), corresponding to immobile Ga atoms. The maximum concentration corresponding to mobile Ga atoms corresponds to $\sim 1 \times 10^{20}$ and 1.3×10^{20} at/cm^3 at 650 and 750°C, respectively (see dashed lines in Fig. 3). This type of observation is common in diffusion profiles. It is generally related to the formation of clusters. The maximum concentration
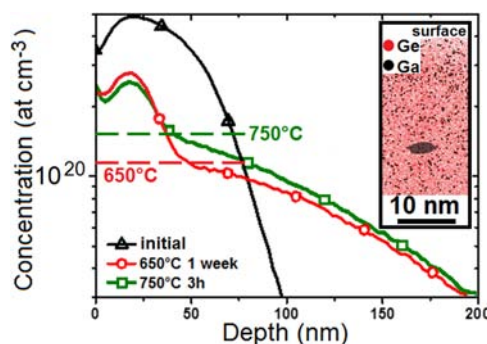

Fig. 3. Gallium SIMS profiles measured in Ge(001) substrate before annealing (triangles) and after annealing at 650°C for 7 days (circles) and at 750°C for 3 h (squares). The inset shows a sample of an APT volume: red and black points correspond to Ge and Ga atoms, respectively. The black volume corresponds to a Ga iso-concentration surface of 3% (Luo et al., 2018). The two dashed lines show the maximum concentrations of mobile Ga at the two different temperatures 650 and 750°C.

of mobile impurities in the SIMS profile measured after annealing corresponds to the solubility limit of the impurity at the corresponding annealing temperature (Portavoce et al., 2004b). One can note that, as expected, the Ga solubility limit determined from the SIMS profiles is found to be higher at 750°C than at 650°C. However, these values are significantly lower than the expected solubility limit of Ga ($\sim 4.5 \times 10^{20}$ at/cm^3) in Ge (Gokhale & Abbaschian, 1990). APT measurements reveal that Ga atoms form disk-shaped accumulations in the sample during diffusion annealing (Luo et al., 2018). The inset in Figure 3 shows a volume of an APT sample measured after annealing at 700°C for 30 min. The red and black dots correspond to Ge and Ga atoms, respectively. The black volume delimited by a 3 at% Ga iso-concentration surface shows one of these Ga accumulations. They contain approximately 3–5 at% Ga and exhibit an average thickness of ~ 2 nm, and an average diameter of ~ 5 nm. Analysis of the atomic density in the Ga accumulation vicinity did not reveal any density variations with respect to the Ge matrix, suggesting that local magnification did not affect the measurements. Figure 4 presents the comparison between a SIMS profile (blue open squares with solid line) and a concentration profile measured by APT (red open triangles) in the vicinity of the immobile Ga distribution in the same sample. The concentration error in the SIMS profiles has been estimated to be $\sim 6\%$ by measuring, several times, the concentration in the same sample with the same experimental conditions. This error is about the size of the square symbols used in the SIMS profile, and thus cannot explain the difference observed between SIMS and APT measurements. The difference between SIMS and APT in the region of immobile Ga (depth <50 nm) could be linked to the SIMS matrix effect related to the Ga accumulations. One can note that SIMS and APT measurements are in quite good agreement for depths between 50 and 100 nm. At depths larger than 100 nm, the concentration measured by APT is found to be lower than in the SIMS profile. These differences can also be linked to the statistical difference between SIMS and APT data, the APT measurement being not representative of the global Ga distribution in the sample due to Ga composition fluctuations related to the distribution of Ga accumulations. However, the comparison between the APT Ga concentration profiles corresponding to the entire Ga distribution (red open triangles) and to the solute Ga atoms (black open squares) confirms that the immobile Ga atoms correspond to the disk-shaped Ga
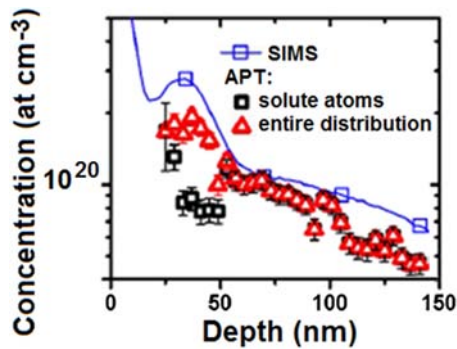
Fig. 4. Comparison between Ga concentration profiles measured by SIMS (squares) and APT (squares for diluted atoms and triangles for the entire Ga distribution) in the same Ga-doped Ge substrate.

Fig. 5. Platinum SIMS profiles measured in a 150 nm-thick polycrystalline Ni_2Si layer sandwiched between two thin SiO_2 layers (<10 nm), before (black solid line), and after (red solid line) diffusion (annealing at 450°C for 1 h).

Fig. 6. Platinum diffusion profiles measured by APT in a 100 nm-thick polycrystalline Ni_2Si layer: in a single grain (solid line), a single GB (solid squares), and a single triple joint (solid triangles) (Portavoce et al., 2012a). The maximum error in the three profiles measured by APT is shown in the figure legend.

accumulations. TEM observations showed that the size and depth location of the Ga-rich defects match the size and depth location of dislocation loops present in the samples (Luo et al., 2018). Thus, the Ga accumulations are not related to the formation of Ga precipitates due to phase separation between Ga and Ge (Gokhale & Abbaschian, 1990), but to Ga segregation on dislocation loops, explaining the observation of Ga accumulations for Ga concentrations below the solubility limit in Ge. The increase of Ga solute atom concentration with temperature is not related to the increase of Ga solubility with temperature, as is usually assumed from the SIMS measurements, but to the usual decrease of the equilibrium segregation driving force when the temperature increases (Portavoce et al., 2004a; Fournier Dit Chabert et al., 2007). In the present case, the diffusion model used to determine the Ga diffusion coefficients from the fit of the experimental SIMS profiles should not include precipitation but segregation on dislocation loops.

Diffusion in polycrystals is complicated by the presence of several diffusion paths such as grains, GBs, and triple junctions (TJs), with different diffusion coefficients (Portavoce et al., 2012b), leading to different kinetic regimes [A, B, and C from Harrison (1961)]. 2D or 3D modeling is needed in order to take into account diffusion in every diffusion path (Portavoce et al., 2008, 2010, 2012b). Furthermore, the mathematical solutions of the diffusion equations used to extract diffusion coefficients from experiments require precise knowledge of the kinetic regime (A, B, or C) in which the diffusion takes place (Harrison, 1961; Gilmer & Farrell, 1976a, 1976b; Mehrer, 2007; Portavoce et al., 2008). SIMS and APT coupling is thus of high interest. SIMS measurements inform on the global distribution of the impurity (Fig. 5) with significant statistics, due to the large lateral length of the analyzed region, and on a significant length scale that can be several microns deep (the larger the diffusion length, the smaller the diffusion coefficient error). While APT allows the impurity diffusion profiles to be measured in a single grain, a single GB, and a single TJ as shown in Figure 6 (Chellali et al., 2011, 2013; Stender et al., 2011). For example, Figure 5 presents the Pt SIMS profiles measured before (black solid line) and after (red solid line) Pt diffusion at 450°C for 1 h in a polycrystalline Ni_2Si layer grew on a SiO_2/Si substrate. The shape of the diffusion profile suggests that Pt diffusion occurred in the kinetic regime B. Indeed, during annealing in this kinetic regime, atoms diffuse simultaneously in grains and GBs. However, the atom diffusion length in grains is significantly larger than the GB width, but significantly smaller than the average grain lateral size. In this case, in a semi-infinite
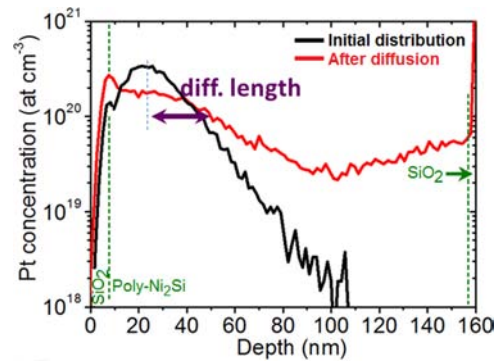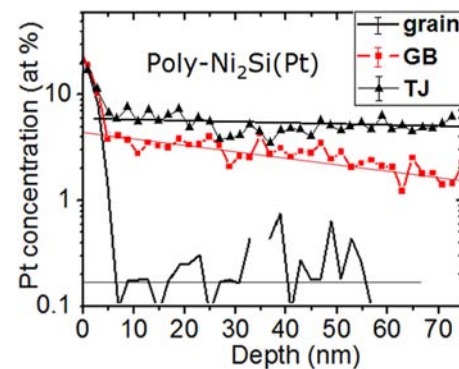
matrix, the diffusion profile exhibits a typical shape with a Gaussian part corresponding to lattice diffusion (in grains), and a linear part corresponding to GB diffusion as well as to diffusion between grains and GBs. This profile can be modified in thin films, since the matrix size is finite and since backward diffusion can also occur in grains once the atoms have reached the film interface via GB diffusion (the interface acts as a second diffusion source). In this case, the profile is similar to the profile shown in Figure 5 for Pt, with a concentration increase close to the Ni_2Si/SiO_2 interface due to the back-diffusion from the interface toward the grains of the layer, resulting from atoms arriving at the interface by GB diffusion (Gilmer & Farrell, 1976a, 1976b; Blum et al., 2008). Thus, the GB diffusion coefficient could be extracted from this diffusion profile using the thin film solution of the 2D Fisher model in the kinetic regime B, without considering Pt cluster formation, since all the Pt atoms seem mobile during annealing (Gilmer & Farrell, 1976a, 1976b). As expected, APT measurements performed in the same sample detected only randomly distributed Pt atoms. However, this random distribution corresponds only to Pt atoms located in the grains of the Ni_2Si layer, showing an almost flat distribution in the entire layer. Figure 7 presents the comparison between the APT 1D profile of these diluted Pt atoms and the SIMS profile. According to the kinetic regime B, the left part of the SIMS profile should correspond to solute Pt atoms located in the grains and exhibiting a slow diffusivity compared to GBs. The lattice diffusion coefficient should be linked to the
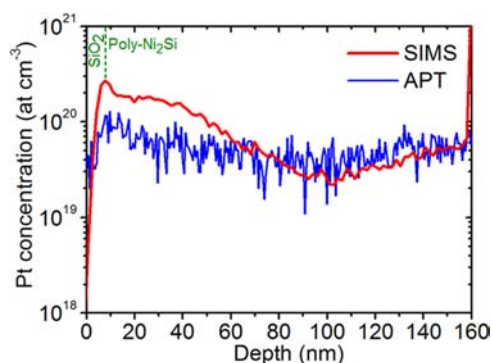
Fig. 7. Comparison between Pt concentration profiles measured by SIMS (red line) and APT (blue line) in the same polycrystalline Ni_2Si layer annealed at 450°C for 1 h after Pt implantation.
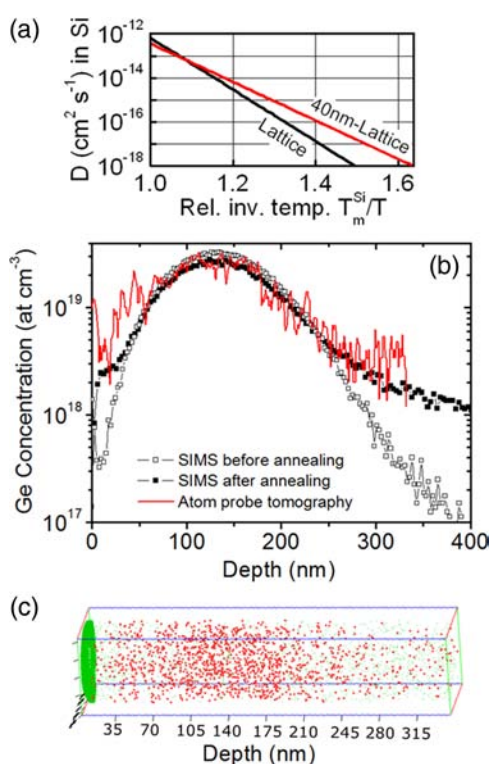

Fig. 8. Experimental data concerning Ge diffusion in nano-crystalline Si (Portavoce et al., 2016): (**a**) comparison between Ge lattice diffusion coefficients in Si macroscopic single crystal (black line) and Si nanocrystal (red line) versus the inverse of temperature (*T*) normalized to the Si melting temperature (T_m^{Si}); (**b**) germanium SIMS profiles measured before (open squares) and after (solid squares) Ge diffusion at 850°C compared with the APT Ge concentration profile measured in the same sample after diffusion (solid line); and (**c**) APT volume corresponding to the Ge concentration profile shown in (**b**), only the Ge atoms are presented (red points). The green points correspond to Ni atoms from the Ni layer deposited at room temperature on the sample surface during FIB sample preparation.

numerical simulations taking into account the experimental initial distribution (black solid line in Fig. 5), the average size of the grains, and the annealing conditions should be able to extract the diffusion coefficients in grains and GBs. The difference between the SIMS and the APT profile closer to the surface could be due to the formation of Pt clusters that were not observed by APT due to a low bulk density.

Figure 8a presents the comparison between the Ge lattice diffusion coefficients measured in Si single crystal (black solid line) and in 40 nm-wide Si nanocrystals (red solid line) (Portavoce et al., 2008, 2010, 2016). Ge diffusion is found to be faster in Si nanocrystals. The diffusion coefficient in nanocrystals was measured in nanocrystalline Si layers using 2D and 3D simulations from the SIMS profiles shown in Figure 8b (Portavoce et al., 2008, 2010, 2016). The part of the profile mainly depending on lattice diffusion is the Gaussian part centered at the depth of 150 nm. Again, SIMS profiles are needed to determine diffusion coefficients, but APT can be used to check the validity of the model used to extract the diffusivities. In the present case, the diffusion kinetic increase of Ge atoms in the Si nano-grains could be related to the presence of diffusion short-circuits located in the grains, such as dislocations for example. In this case, the Ge distribution in the grains should be modified by the defects and the Ge distribution should not be random. Figure 8c presents an APT volume measured after annealing in the sample in which the SIMS profile (solid squares) presented in Figure 8b was measured. The distance separating the SIMS crater from the region analyzed by APT was ~0.3 cm. Only the Ge atoms (red points) are presented. The section of the volume is 40×40 nm^2 corresponding to the average lateral size of the Si nano-grains, and its depth is larger than 300 nm. Ge atoms are randomly distributed in the volume, no sign of defect-mediated Ge fast diffusion was detected (Portavoce et al., 2017). The corresponding APT profile is in good agreement with the SIMS profile (Fig. 8b), in particular in the region where the profile variations are mainly controlled by lattice diffusion. Consequently, APT measurements confirm the validity of the 2D and 3D models used to measure the Ge diffusion coefficients, suggesting a real lattice diffusion enhancement in Si nano-grains, probably due to an increase of vacancy concentration in Si nanocrystals (Portavoce et al., 2017).

Polycrystalline material properties (e.g., mechanical, electrical) can significantly depend on the impurity segregation at GBs. It is thus important to be able to quantify the concentration of GB segregating impurities. Furthermore, segregation coefficients and segregation activation energy measurements are used to predict the influence of processing and aging on material properties. APT measurements give access to 1D, 2D, and 3D atomic distributions, allowing quantitative concentration measurements in extended defects such as GBs and dislocations (Blavette et al., 1999; Seol et al., 2011, 2013). For example, Figure 9a shows a 2D Pt concentration map in a polycrystalline Ni_2Si layer. The difference of Pt concentrations among Ni_2Si grains (dark blue surfaces), GBs (light blue lines), and TJs (yellow-red peaks) is obvious (Portavoce et al., 2012b). The concentration ratio between grain and GB (segregation coefficient) can easily be measured using the 1D profile (Fig. 9b) determined along the red line shown in Figure 9a. However, equilibrium segregation isotherms are usually characterized by high segregation concentrations in defects for low bulk concentrations (Eugène et al., 1991). APT appears to be a suitable technique for measuring segregation concentrations in GBs (Seol et al., 2011, 2013), but its detection limit may be too high for measuring the bulk concentration (in grains)

diffusion length shown in Figure 5 (purple line), determined from the comparison between the profiles measured before and after annealing. However, the APT profile shows that the solute Pt atoms diffused through the entire layer, and that the Gaussian distribution on the left does not correspond to diluted Pt atoms located in grains. Consequently, the SIMS profile does not correspond to diffusion kinetic regime B. The diffusion solution of the kinetic regime B should not be used in this case. Only 2D
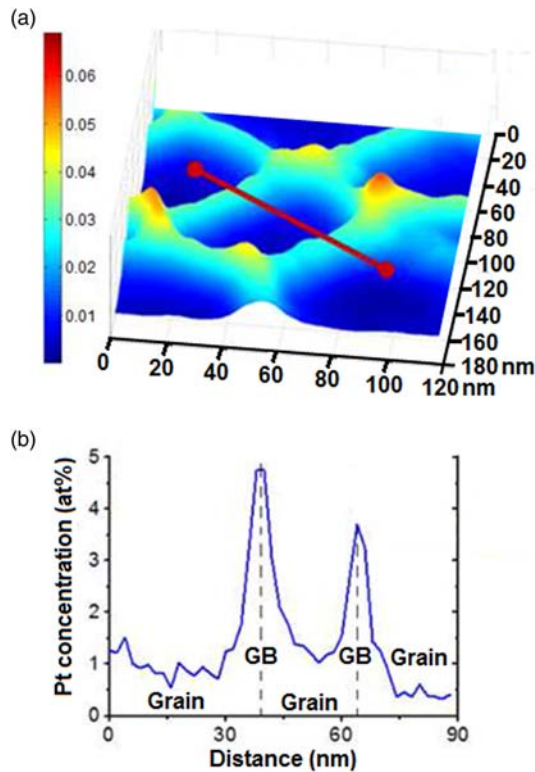
Fig. 9. Experimental Pt distribution determined by APT at a given depth in a polycrystalline Ni_2Si layer: (**a**) 2D distribution, and (**b**) Pt concentration along the red line shown in (**a**) (Portavoce, 2012a).

in equilibrium with the GB concentration. In contrast, SIMS measurements allow low bulk concentration measurements, but are not quantitative in GBs due to matrix effects. Thus, nano-SIMS and APT coupling seems to be a worthwhile solution for study GB equilibrium segregation. Indeed, APT can be used to calibrate the nano-SIMS intensity in the case of higher bulk concentrations, in order to use nano-SIMS to measure bulk concentration in equilibrium with GB segregation concentration, the GB concentration being measured by APT.

Summary

Due to the substantial scale difference between SIMS (micrometric scale) and APT (atomic scale) data, correlative SIMS and APT measurements offer significant benefits for atomic redistribution studies (diffusion, segregation, precipitation, etc.). APT can be used to confirm the reliability of SIMS profiles (matrix effect, mixing effect, etc.), as well as to validate the consistency of the diffusion models (kinetic regimes, boundary conditions, etc.) used to measure diffusion coefficients from SIMS profiles. APT allows the accuracy of these diffusion models (clusters analysis, contribution of grain and GB distributions in the global diffusion profile, etc.) to be improved thanks to its atomic resolution. In the case of polycrystalline materials, coupling SIMS and APT measurements allows the global atomic distribution measured by SIMS and the local GB and grain distributions measured by APT to be compared, bringing an interesting outlook on atomic transport mechanisms. Furthermore, correlative nano-SIMS and APT measurements offer the possibility to study equilibrium GB segregation in the case of very diluted solid solutions.

References

Aboulfadl H, Seifried F, Stüber M & Mücklich F (2019). Interdiffusion in as-deposited Ni/Ti multilayer thin films analyzed by atom probe tomography. *Mater Lett* **236**, 92–95.

Benninghoven A, Rüdenauer FG & Werner HW (1987). *Secondary Ion Mass Spectrometry: Basic Concepts, Instrumental Aspects, Applications, and Trends*. New York, USA: Wiley.

Blavette D, Cadel E, Fraczkiewicz A & Menand A (1999). Three-dimensional atomic-scale imaging of impurity segregation to line defects. *Science* **286**, 2317–2319.

Blum I, Portavoce A, Mangelinck D, Daineche R, Hoummada K, Lábár JL, Carron V & Perrin C (2008). Lattice and grain-boundary diffusion of As in Ni_2Si. *J Appl Phys* **104**, 114312.

Chellali MR, Balogh Z & Schmitz G (2013). Nano-analysis of grain boundary and triple junction transport in nanocrystalline Ni/Cu. *Ultramicroscopy* **132**, 164–170.

Chellali MR, Balogh Z, Zheng L & Schmitz G (2011). Triple junction and grain boundary diffusion in the Ni/Cu system. *Scripta Mater* **65**, 343–346.

De Luca A, Portavoce A, Texier M, Grosjean C, Burle N, Oison V & Pichaud B (2014). Tungsten diffusion in silicon. *J Appl Phys* **115**, 013501.

Eugène J, Aufray B & Cabané F (1991). Equilibrium of segregation in Ag/Cu (111): Kinetics and isotherms. *Surf Sci* **241**, l–5.

Fournier Dit Chabert F, Tancret F, Christien F, Le Gall R & Castagne J-F (2007). Finite element simulation of interfacial segregation in dilute alloys. *J Mater Sci* **42**, 9765–9774.

Gilmer GH & Farrell HH (1976a). Grain-boundary diffusion in thin films. I. The isolated grain boundary. *J Appl Phys* **47**, 3792–3798.

Gilmer GH & Farrell HH (1976b). Grain-boundary diffusion in thin films. II. Multiple grain boundaries and surface diffusion. *J Appl Phys* **47**, 4373–4380.

Gokhale A & Abbaschian GJ (1990). *Binary Alloy Phase Diagrams*. ASM International: www.asminternational.org.

Harrison LG (1961). Influence of dislocations on diffusion kinetics in solids with particular reference to the alkali halides. *Trans Faraday Soc* **57**, 1191–1199.

Kresse T, Li YJ, Boll T, Borchers C, Choi P, Al-Kassab T, Raabeb D & Kirchheim R (2013) Influence of supersaturated carbon on the diffusion of Ni in ferrite determined by atom probe tomography. *Scripta Mater* **69**, 424–427.

Larson DJ, Prosa TyJ, Ulfig RM, Geiser BP & Kelly TF (2013). *Local Electrode Atom Probe Tomography*. New York, USA: Springer.

Luo T, Perrin Toinin J, Descoins M, Hoummada K, Bertoglio M, Chow L, Narducci D & Portavoce A (2018). PdGe contact fabrication on Ga-doped Ge: Influence of implantation-mediated defects. *Scripta Mater* **150**, 66–69.

Martinez E, Ronsheim P, Barnes J-P, Rochat N, Pya M, Hatzistergos M, Renault O, Silly M, Sirotti F, Bertin F & Gambacorti N (2011). Lanthanum diffusion in the $TiN/LaOx/HfSiO/SiO_2/Si$ stack. *Microelec Eng* **88**, 1349–1352.

Mehrer H (2007). *Diffusion in Solids*. Berlin, Germany: Springer-Verlag.

Mühlbacher M, Mendez-Martina F, Sartory B, Schalka N, Keckes J, Lu J, Hultman L & Mitterer C (2015). Copper diffusion into single-crystalline TiN studied by transmission electron microscopy and atom probe tomography. *Thin Solid Films* **574**, 103–109.

Portavoce A, Abbes O, Rudzevich Y, Chow L, Le Thanh V & Girardeaux C (2012a). Manganese diffusion in monocrystalline germanium. *Scripta Mater* **67**, 269–272.

Portavoce A, Berbezier I, Gas P & Ronda A (2004a). Sb surface segregation during epitaxial growth of SiGe heterostructures: The effects of Ge composition and biaxial stress. *Phys Rev B* **69**, 155414.

Portavoce A, Blum I, Hoummada K, Mangelinck D, Chow L & Bernardini J (2012b). Original methods for diffusion measurements in polycrystalline thin films. *Defect Diffusion Forum* **322**, 129–150.

Portavoce A, Chai G, Chow L & Bernardini J (2008). Nanometric size effect on Ge diffusion in polycrystalline Si. *J Apply Phys* **104**, 104910.

Portavoce A, Chow L & Bernardini J (2010). Triple-junction contribution to diffusion in nanocrystalline Si. *Appl Phys Lett* **96**, 214102.

Portavoce A, Gas P, Berbezier I, Ronda A, Christensen JS, Kuznetsov AYu & Svensson BG (2004*b*). Sb lattice diffusion in $Si_{1-x}Ge_x/Si(001)$ hetero-structures: Chemical and stress effects. *Phys Rev B* **69**, 155415.

Portavoce A, Hoummada K & Chow L (2016). Atomic transport in nano-crystalline thin films. *Defect Diffusion Forum* **367**, 140–148.

Portavoce A, Hoummada K, Ronda A, Mangelinck D & Berbezier I (2014). Si/Ge intermixing during Ge Stranski–Krastanov growth. *Beilstein J Nanotechnol* **5**, 2374–2382.

Portavoce A, Perrin-Toinin J & Hoummada K (2017). Vacancy-mediated atomic transport in nano-crystals. *Rev Adv Mater Sci* **50**, 69–75.

Portavoce A, Rodriguez N, Daineche R, Grosjean C & Girardeaux C (2009). Correction of secondary ion mass spectrometry profiles for atom diffusion measurements. *Mater Lett* **63**, 676–678.

Ronsheim P, Flaitz P, Hatzistergos M, Molella C, Thompson K & Alvis R (2008). Impurity measurements in silicon with D-SIMS and atom probe tomography. *Appl Surf Sci* **255**, 1547–1550.

Saha B & Chakraborty P (2013). MCs_n^+-SIMS: An innovative approach for direct compositional analysis of materials without standards. *Energy Procedia* **41**, 80–109.

Seol JB, Lee B-H, Choi P, Lee S-G & Park C-G (2013). Combined nano-SIMS/AFM/EBSD analysis and atom probe tomography, of carbon distribution in austenite/ε-martensite high-Mn steels. *Ultramicroscopy* **132**, 248–257.

Seol JB, Lim NS, Lee BH, Renaud L & Park CG (2011). Atom probe tomography and nano secondary ion mass spectroscopy investigation of the segregation of boron at austenite grain boundaries in 0.5 wt.% carbon steels. *Met Mater Int* **17**, 413–416.

Sha G & Cerezo A (2005). Field ion microscopy and 3-d atom probe analysis of Al_3Zr particles in 7050 Al alloy. *Ultramicroscopy* **102**, 151–159.

Stender P, Balogh Z & Schmitz G (2011). Triple line diffusion in nano-crystalline Fe/Cr and its impact on thermal stability. *Ultramicroscopy* **111**, 524–529.

Südkamp T, Bracht H, Impellizzeri G, Lundsgaard Hansen J, Nylandsted Larsen A & Haller EE (2013). Doping dependence of self-diffusion in germanium and the charge states of vacancies. *Appl Phys Lett* **102**, 242103.

Toyama T, Takahama F, Kuramoto A, Takamizawa H, Nozawa Y, Ebisawa N, Shimodaira M, Shimizu Y, Inoue K & Nagai Y (2014). The diffusivity and solubility of copper in ferromagnetic iron at lower temperatures studied by atom probe tomography. *Scripta Mater* **83**, 5–8.

Vurpillot F, Bostel A & Blavette D (2000). Trajectory overlaps and local magnification in three-dimensional atom probe. *Appl Phys Lett* **76**, 3127.

Yan Y, Pennycook SJ, Xu Z & Viehland D (1998). Determination of the ordered structures of $Pb(Mg_{1/3}Nb_{2/3})O_3$ and $Ba(Mg_{1/3}Nb_{2/3})O_3$ by atomic-resolution Z-contrast imaging. *Appl Phys Lett* **72**, 3145–3147.

Zalm PC & Vriezema CJ (1992). On some factors limiting depth resolution during SIMS profiling. *Nucl Inst Meth Phys Res* **B67**, 495–499.